

THREE-DIMENSIONAL EXPLOSION GEOMETRY OF STRIPPED-ENVELOPE CORE-COLLAPSE SUPERNOVAE. I. SPECTROPOLARIMETRIC OBSERVATIONS*

MASAOMI TANAKA^{1,2}, KOJI S. KAWABATA³, TAKASHI HATTORI⁴, PAOLO A. MAZZALI^{5,6}, KENTARO AOKI⁴, MASANORI IYE¹, KEIICHI MAEDA², KEN'ICHI NOMOTO², ELENA PIAN⁷, TOSHIYUKI SASAKI⁴, AND MASAYUKI YAMANAKA^{3,8}

¹ National Astronomical Observatory, Mitaka, Tokyo, Japan; masaomi.tanaka@nao.ac.jp

² Institute for the Physics and Mathematics of the Universe, University of Tokyo, Kashiwa, Japan

³ Hiroshima Astrophysical Science Center, Hiroshima University, Higashi-Hiroshima, Hiroshima, Japan

⁴ Subaru Telescope, National Astronomical Observatory of Japan, Hilo, HI 96720, USA

⁵ Max-Planck Institut für Astrophysik, Karl-Schwarzschild-Strasse 2 D-85748 Garching bei München, Germany

⁶ Istituto Naz. di Astrofisica-Oss. Astron., vicolo dell'Osservatorio, 5, 35122 Padova, Italy

⁷ Istituto Naz. di Astrofisica-Oss. Astron., Via Tiepolo, 11, 34131 Trieste, Italy

⁸ Department of Physical Science, Hiroshima University, Higashi-Hiroshima, Hiroshima, Japan

Received 2012 April 5; accepted 2012 May 18; published 2012 July 6

ABSTRACT

We study the multi-dimensional geometry of supernova (SN) explosions by means of spectropolarimetric observations of stripped-envelope SNe, i.e., SNe without a hydrogen-rich layer. We perform spectropolarimetric observations of two stripped-envelope SNe, Type Ib SN 2009jf and Type Ic SN 2009mi. Both objects show non-zero polarization at the wavelength of the strong lines. They also show a loop in the Stokes $Q-U$ diagram, which indicates a non-axisymmetric, three-dimensional ion distribution in the ejecta. We show that five out of six stripped-envelope SNe, which have been observed spectropolarimetrically so far, show such a loop. This implies that a three-dimensional geometry is common in stripped-envelope SNe. We find that stronger lines tend to show higher polarization. This effect is not related to the geometry, and must be corrected for to compare the polarization of different lines or different objects. Even after the correction, however, there remains a dispersion of polarization degree among different objects. Such a dispersion might be caused by three-dimensional clumpy ion distributions viewed from different directions.

Key words: supernovae: general – supernovae: individual (SNe 2009jf, 2009mi) – techniques: polarimetric

Online-only material: color figures

1. INTRODUCTION

1.1. Explosion Geometry of Supernovae

Core-collapse supernovae (SNe) are the explosions of massive stars at the end of their lives. Besides their importance as the end points of stellar evolution, SNe play an important role in the chemical and dynamical evolution of galaxies. However, the explosion mechanism of SNe has been unclear for a long time after the first concept proposed by Burbidge et al. (1957) and the first numerical simulation by Colgate & White (1966).

Modern detailed numerical simulations agree in that a successful explosion cannot be obtained in one-dimensional (1D) simulations (Rampp & Janka 2000; Liebendörfer et al. 2001; Thompson et al. 2003; Sumiyoshi et al. 2005). Recently, increasing attention is being paid to multi-dimensional effects, such as convection (e.g., Herant et al. 1994; Burrows et al. 1995; Janka & Mueller 1996) and Standing Accretion Shock Instability (e.g., Blondin et al. 2003; Scheck et al. 2004; Ohnishi et al. 2006; Fogliizzo et al. 2007; Iwakami et al. 2008). In fact, some successful explosions have been obtained in two-dimensional (2D) simulations (Buras et al. 2006; Marek & Janka 2009; Suwa et al. 2010).

Thanks to the advancements in numerical simulations, some simulations have been done in a fully three-dimensional (3D) space (Nordhaus et al. 2010; Wongwathanarat et al. 2010; Takiwaki et al. 2012; Kuroda et al. 2012). Interestingly,

Nordhaus et al. (2010) show that it is easier to obtain a successful explosion in 3D simulations than in 2D simulations (but see also Hanke et al. 2011).

Given these circumstances, it is important to obtain observational constraints on the multi-dimensional geometry of SN explosions. The most direct way is the observation of spatially resolved SNe. Isensee et al. (2010) and DeLaney et al. (2010) performed detailed observations of the Galactic SN remnant Cassiopeia A. Using a combination of imaging and spatially resolved spectroscopy, they reconstructed the 3D geometry of the SN. Similarly, direct imaging (Wang et al. 2002) and spatially resolved spectroscopy (Kjær et al. 2010) have been performed for SN 1987A in the Large Magellanic Cloud. However, the number of objects suitable for such observations is limited.

Observations of extragalactic SNe can also provide hints of explosion geometry, although at this distance SNe are point sources. For example, spectroscopic observations of SNe at >1 yr after the explosion provide information of explosion geometry. At such late epochs, SN ejecta are optically thin. Therefore, this method is sensitive to the geometry of the innermost ejecta. By analyzing line profiles of nebular emission, a bipolar geometry of SNe has been suggested (e.g., Mazzali et al. 2001, 2005; Maeda et al. 2002, 2008; Modjaz et al. 2008; Tanaka et al. 2009b; Taubenberger et al. 2009; Maurer et al. 2010, but see also Milisavljevic et al. 2010).

Polarization at early phases ($\lesssim 50$ days after the explosion) is another powerful method for studying the multi-dimensional geometry of extragalactic SNe (see Wang & Wheeler 2008 for a review). In contrast to late phase spectroscopy, polarization is sensitive to the geometry of the outer ejecta. In particular,

* Based on data collected at Subaru Telescope, which is operated by the National Astronomical Observatory of Japan.

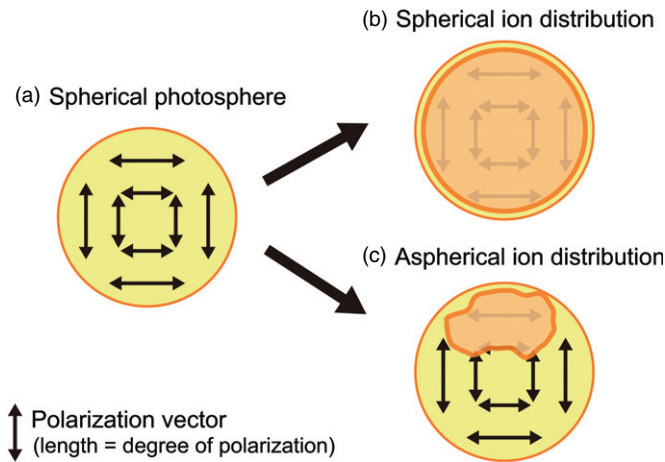


Figure 1. Schematic illustration of polarization in the SN ejecta (see also Kasen et al. 2003; Leonard & Filippenko 2005; Wang & Wheeler 2008). (a) When the photosphere is spherical, polarization is canceled out, and no polarization is expected. At the wavelength of a line, polarization produced by the electron scattering is depolarized by the line transition. (b) When the ion distribution is spherical, the remaining polarization is canceled, and no polarization is expected. (c) When the ion distribution is not spherical, the cancellation becomes incomplete, and line polarization could be detected (e.g., Jeffery 1989; Kasen et al. 2003; Wang & Wheeler 2008).

(A color version of this figure is available in the online journal.)

spectropolarimetry can probe 3D geometry, as explained in the following section. In this paper, we study the multi-dimensional explosion geometry of SNe using spectropolarimetric observations.

1.2. Power of Spectropolarimetry

Polarization in SNe is generated by electron scattering. Since the polarization degree of the scattered light reaches its maximum when the scattering angle is 90° , the expected polarization map for a spherical photosphere looks like (a) in Figure 1. However, SNe are observed as point sources, and thus all the polarization vectors cancel out, resulting in no polarization.⁹

Absorption and re-emission by a bound-bound transition, which create a P-Cygni profile in the expanding ejecta, tend to cause depolarization (Jeffery 1989; Kasen et al. 2003). Thus, the polarization produced by the electron scattering is effectively concealed by the interaction with lines. If an ion is distributed spherically (b), polarization vectors still cancel out, and no polarization is expected at the wavelength of the line. Polarization would be detected at the wavelength of the absorption line only if the ion is distributed asymmetrically (c), because of the incomplete cancellation. Thus, we can identify an asymmetric ion distribution by detecting line polarization.

Note that an asymmetric ion distribution is expected either from an asymmetric element distribution, which could be produced by a multi-dimensional explosion (e.g., Nagataki et al. 1997; Kifonidis et al. 2000, 2003; Maeda et al. 2003; Tominaga 2009; Fujimoto et al. 2011), or by an asymmetric ionization/temperature structure, which is caused by an asymmetric distribution of ^{56}Ni (Tanaka et al. 2007).

⁹ When the photosphere is deformed, the cancellation of polarization becomes incomplete. As a result, continuum polarization will be detected (Shapiro & Sutherland 1982; Höflich 1991). Although continuum polarization is difficult to distinguish from interstellar polarization, multi-epoch observations have revealed that there is non-zero continuum polarization in Type IIP SNe after the plateau phase (Leonard et al. 2006; Chornock et al. 2010).

The properties of linear polarization are fully described by the Stokes parameters. Throughout this paper, we define the Stokes parameters as a fraction of the total flux: $Q \equiv \hat{Q}/I$ and $U \equiv \hat{U}/I$, where \hat{Q} and \hat{U} can be expressed as $\hat{Q} = I_0 - I_{90}$ and $\hat{U} = I_{45} - I_{135}$, respectively. Here I_θ is the intensity measured through the ideal polarization filter with an angle θ . From the Stokes parameters Q and U , the polarization position angle θ is obtained by

$$2\theta = \text{atan}(U/Q). \quad (1)$$

The position angle is measured from north to east in the sky.

Figure 2 shows the expected line polarization in a 2D bipolar model (top) and a 3D clumpy model (bottom). The polarization spectra are calculated by the Monte Carlo method for arbitrary line optical depth distributions, under assumptions similar to those in Kasen et al. (2003) and Hole et al. (2010). The details of the simulations will be given in a forthcoming paper. The left panels show the distribution of line optical depth. In the 2D model, the opacity is enhanced by a factor of 10 in the polar region, while in the 3D model, the opacity is similarly enhanced in the randomly distributed clumps.

In both cases, the polarization changes at the wavelength of the line (middle panels), which is caused by the asymmetric distribution of the line optical depth. However, the behavior of the polarization angle is different. In the 2D case, the polarization angle is constant (some fluctuation is caused by the Monte Carlo noise), while in the 3D case, it largely changes across the line. Since the SN ejecta expand homologously and the velocity can be used as a radial coordinate, a change in the polarization angle means a radially dependent ion distribution.

This effect is more clearly seen in the $Q-U$ plane. The right panels in Figure 2 show the same simulated polarization spectrum in the $Q-U$ plane. Different colors represent different Doppler velocities, according to the color bar above the plots. The polarization for the 2D model shows a straight line in the $Q-U$ plane, while that for the 3D model shows a “loop,” which corresponds to a change in the polarization angle.

Therefore, a change in the polarization angle or the loop in the $Q-U$ plane is indicative of a 3D ion distribution. In order to fully utilize the power of spectropolarimetry, we should obtain high-quality data to discriminate such a feature from noise. Loops in the $Q-U$ plane have been commonly observed in Type Ia SNe (Wang et al. 2003a; Kasen et al. 2003; Chornock & Filippenko 2008; Patat et al. 2009) and in some core-collapse SNe (e.g., Maund et al. 2007b, 2007c, 2009).

1.3. This Paper

In this paper, we show our spectropolarimetric observations of two Type Ib/c SNe with the Subaru Telescope (Sections 2 and 3). The first target is the Type Ib SN 2009jf (discovered in NGC 7479 by Li et al. 2009 on UT 2009 September 27.33 and classified by Kasliwal et al. 2009; Sahu et al. 2009). See Sahu et al. (2011) and Valenti et al. (2011) for more details. The other target is the Type Ic SN 2009mi (discovered in IC 2151 by Monard et al. 2009 on UT 2009 December 12.91 and classified by Kinugasa et al. 2009).

We then summarize the spectropolarimetric data of stripped-envelope SNe published so far (Section 4). We argue that a non-axisymmetric, 3D geometry is common in stripped-envelope SNe. We find a relation between line polarization and the depth of absorptions: i.e., a stronger line tends to show a higher line polarization. Even after correcting for the effect of the absorption depth, there remains a dispersion in the

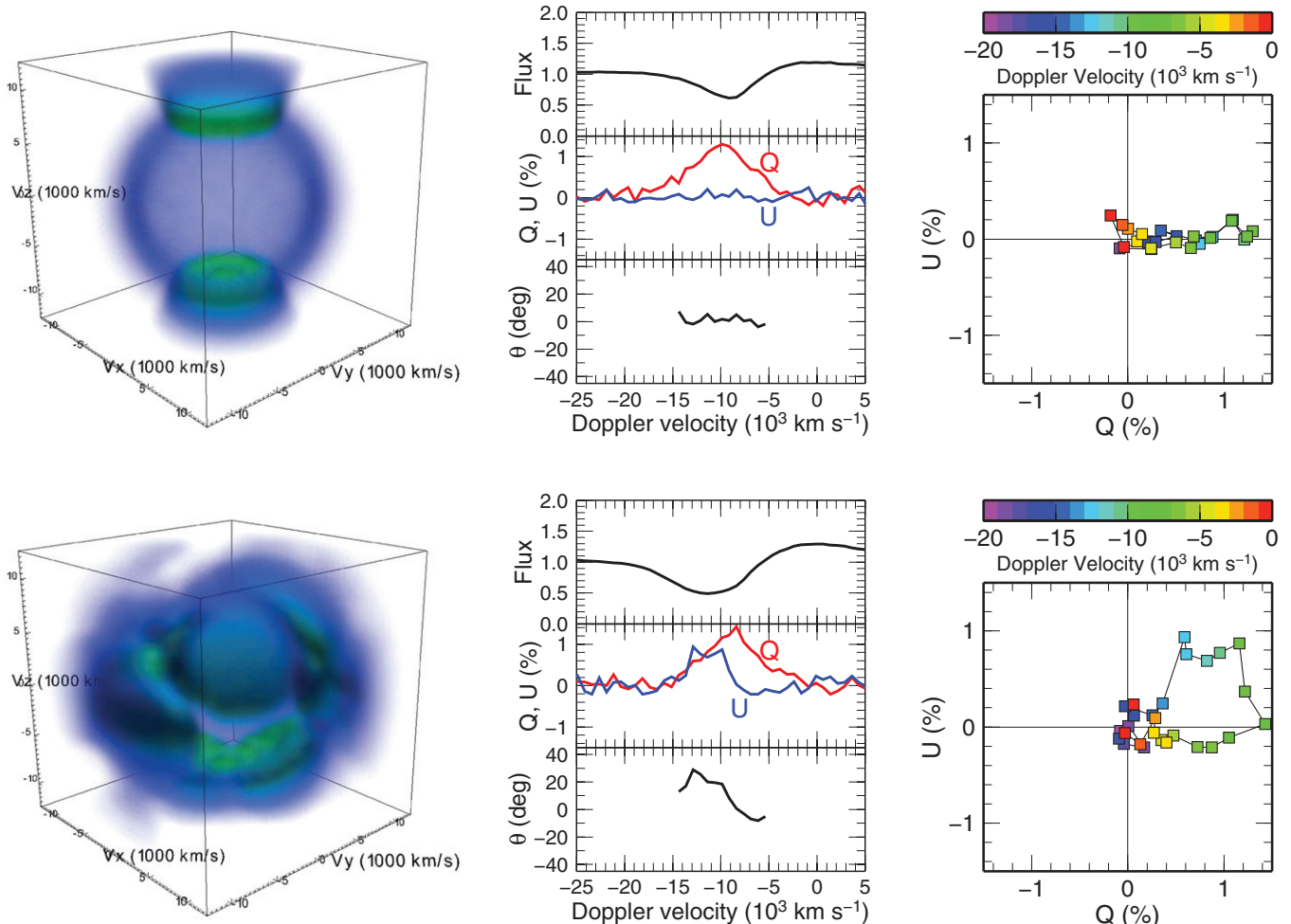


Figure 2. Simulated line polarization for a 2D bipolar model (top) and a 3D clumpy model (bottom). Left: the distribution of the line optical depth. Middle: the total flux spectrum and polarization spectrum. The polarization angle is consistent with a constant in the 2D model, while it changes across the line in the 3D model. Right: the same simulated polarization but in the $Q-U$ diagram. Different colors represent different Doppler velocities, according to the color bar above the plots. The polarization data show a straight line (constant angle) in the 2D model, while the data show a loop (variable angle) in the 3D model. Details of the simulations will be given in a forthcoming paper.

(A color version of this figure is available in the online journal.)

polarization degree among different objects. The implications of this dispersion are discussed. Finally, we give conclusions in Section 5.

2. OBSERVATIONS

We have performed spectropolarimetric observations of SNe 2009jf and 2009mi with the 8.2 m Subaru Telescope equipped with the Faint Object Camera and Spectrograph (Kashikawa et al. 2002) on UT 2009 October 24.3 (MJD = 55128.3) and 2010 January 8.3 (MJD = 55204.3), respectively. These epochs correspond to $t = +9.3$ and $+26.5$ days from the B -band maximum (MJD = 55118.96 for SN 2009jf according to Sahu et al. 2011, and MJD = 55177.8 for SN 2009mi, based on our observations). Hereafter, t denotes the days after the B -band maximum. The log of observations are shown in Table 1.

For both observations, we used an offset slit of $0''.8$ width, a $300 \text{ lines mm}^{-1}$ grism, and the Y47 filter. This configuration gives a wavelength coverage of $4700\text{--}9000 \text{ \AA}$. The wavelength resolution is $\Delta\lambda \simeq 10 \text{ \AA}$. For the measurement of linear polarization, we use a rotating superachromatic half-wave plate and a crystal quartz Wollaston prism. One set of observations consists of the integrations with the 0° , 45° , 22.5° , and 67.5°

positions of the half-wave plate. From this set of exposures, the Stokes parameters Q and U are derived as described by Tinbergen (1996).

For the observations of SN 2009jf we performed six sets of the integrations at the four angles with a total exposure time of 4.0 hr. For SN 2009mi, we performed five sets of the integrations at the four angles with a total exposure time of 3.8 hr. Typical seeing during the observations was $0''.8$ and $1''.1\text{--}1''.5$ for SNe 2009jf and 2009mi, respectively.

After deriving the Stokes parameters for each set of observations, these were combined. Then, the instrumental polarization ($\sim 0\%\text{--}0.4\%$) was evaluated and subtracted using unpolarized stars (Schmidt et al. 1992), G191-B2B (for both objects), BD+28 $^\circ$ 4211 (for SN 2009jf), and HD 14069 (for SN 2009mi), observed on the same night. The reference axis of the position angle was calibrated by the observation of the strongly polarized star Hiltner 960 (Schmidt et al. 1992 for SN 2009jf) and HD 251204 (Turnshek et al. 1990 for SN 2009mi). The wavelength dependence of the optical axis of the half-wave plate was corrected using the dome flat taken through a fully polarizing filter. The total flux was calibrated using the observation of the spectrophotometric standard stars BD+28 $^\circ$ 4211 and G191-B2B

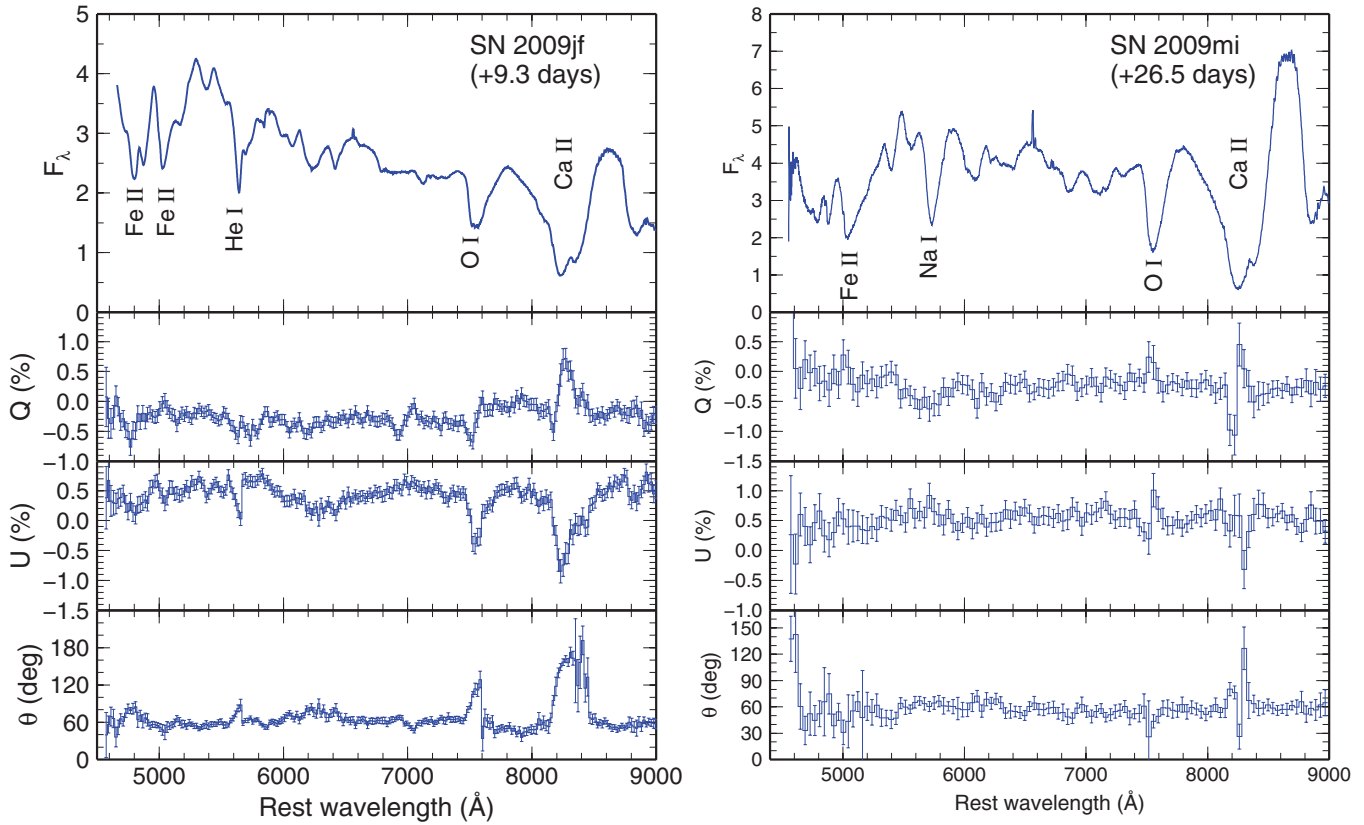


Figure 3. Total flux spectrum and polarization spectrum of SNe 2009jf (left) and 2009mi (right). The total flux is shown in units of 10^{-15} and 10^{-16} $\text{erg s}^{-1} \text{cm}^{-2} \text{\AA}^{-1}$ for SNe 2009jf and 2009mi, respectively. The polarization data are binned into 25 and 50 \AA for SNe 2009jf and 2009mi, respectively. In the plot of Stokes parameters and the polarization angle, the contribution of the interstellar polarization is *not* corrected for.

(A color version of this figure is available in the online journal.)

Table 1
Log of Observations

Object	Date (UT)	Date (MJD)	Exposure Time (s)	Airmass	Comment
SN 2009jf (+9.3 d)	2009 Oct 24.3	55128.3	$(600 \times 4) \times 6$	1.03–1.43	SN
BD+28°4211	2009 Oct 24.2	55128.2	$(20 \times 4) + (40 \times 4)$	1.01	Unpolarized/flux std.
G191-B2B	2009 Oct 24.6	55128.6	$(60 \times 4) \times 2$	1.33	Unpolarized std.
Hiltner 960	2009 Oct 24.2	55128.2	20×4	1.08	Polarized std.
SN 2009mi (+26.5 d)	2010 Jan 8.3	55204.3	$(600 \times 4) + (1000 \times 4)$	1.26–1.83	SN
G191-B2B	2010 Jan 8.2	55204.2	$(60 \times 4) \times 2$	1.43	Unpolarized/flux std.
HD 14069	2010 Jan 8.2	55204.2	$(5 \times 4) \times 2$	1.03	Unpolarized std.
HD 251204	2010 Jan 8.2	55204.2	20×4	1.48	Polarized std.

Note. All the observations were performed with a $0''.8$ width offset slit, a 300 lines mm^{-1} grism, and the Y47 filter, giving the wavelength coverage 4700–9000 \AA and the wavelength resolution $\Delta\lambda \simeq 10 \text{\AA}$.

(Massey et al. 1988; Massey & Gronwall 1990; Oke 1990) for SNe 2009jf and 2009mi, respectively. Telluric absorption lines were also removed using the spectrum of these standard stars.

3. RESULTS

Figure 3 shows the observed total flux and polarization spectra of SNe 2009jf and 2009mi. The observed polarization is the sum of the intrinsic and interstellar polarization (ISP). ISP is caused by interstellar dust both in our Galaxy and in the host galaxy. However, since the wavelength dependence of the ISP is smooth (Serkowski et al. 1975), the changes in the polarization at the strong absorption lines, such as He I, O I, and Ca II, are certainly

intrinsic. These features clearly indicate a broken symmetry of the SNe.

The same data are shown in the $Q-U$ diagram in Figure 4. Different colors represent different wavelengths, according to the color bar above the plots. Most of the data points, except for the strong lines, are located around $(Q_0, U_0) \simeq (-0.25\%, 0.50\%)$ and $(-0.30\%, 0.60\%)$ for SNe 2009jf and 2009mi, respectively. The spectropolarimetric type is N1 according to the classification scheme of Wang & Wheeler (2008). Some deviation from the reference point could be due to the non-zero continuum polarization of SNe. Hereafter, we use these (Q_0, U_0) as a reference point. This component is most likely to be the ISP for the following reason. The ISP can be corrected if we

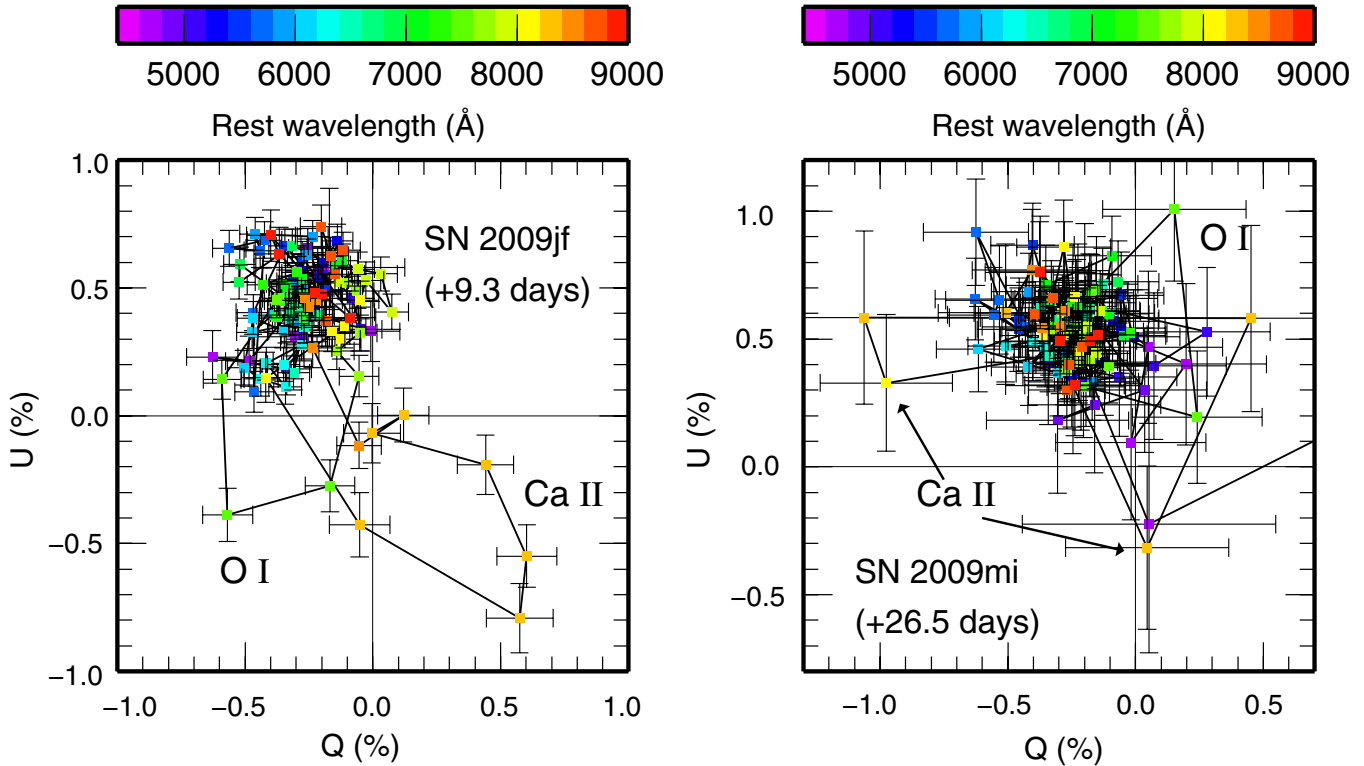


Figure 4. Observed polarization data of SNe 2009jf (left) and 2009mi (right) in the $Q-U$ plane. The polarization data are binned into 50 \AA . The interstellar polarization is *not* corrected for. Different colors show different wavelengths as shown in the color bar above the plots. The polarization data at the O I and Ca II lines are also shown as a function of the Doppler velocity in Figure 5.

(A color version of this figure is available in the online journal.)

assume a complete depolarization at strong emission lines (e.g., Kawabata et al. 2002; Leonard et al. 2005; Wang et al. 2006; Maund et al. 2007a, 2007b). This method is justified because the emission part of a P-Cygni profile consists largely of line-scattered, depolarized photons. In our data, the polarization at the strong emission peak at the Ca II line is consistent with the reference point above. In the following discussion, however, we do not explicitly assume this component to be the ISP but focus only on the line polarization.

The $Q-U$ diagram (Figure 4) is a more unambiguous way to show the observed polarization data than a plot as a function of wavelength (Figure 3). Since the ISP could add an offset to the SN polarization, the polarization angle θ in Figure 3 is not directly related to the SN properties. Instead, one can readily measure the polarization angle θ' from the reference point (Q_0, U_0):

$$2\theta' = \text{atan}[(U - U_0)/(Q - Q_0)]. \quad (2)$$

In Figure 5, we show the data only around the O I and Ca II lines as a function of the Doppler velocity. It is clear that the data at the Ca II and O I lines occupy different regions in the $Q-U$ diagram, indicating different spatial distributions between Ca II and O I. Such a difference is also clearly seen in other SNe, e.g., Type Ib SN 2008D (Maund et al. 2009) and Type IIb SN 2008ax (Chornock et al. 2011).

A more interesting feature is the shape of the polarization data in the $Q-U$ diagram. Starting from the reference point, the Ca II and O I lines in SN 2009jf show a loop at these lines (spectropolarimetric type L). This means that the angle θ' , measured from the reference, varies with the Doppler velocity and the depth in the ejecta (homologous expansion, $r = vt$). As shown in Figure 2, and as suggested by, e.g., Kasen et al. (2003)

and Maund et al. (2007b, 2007c), this loop clearly indicates that even axisymmetry is broken in the SN ejecta.

The Ca II feature of SN 2009mi is even more intriguing. Measuring from the reference point, the variation in the angle θ' is as large as $\sim 90^\circ$ (the difference of 180° in the $Q-U$ diagram corresponds to the difference of 90° in the polarization angle on the sky). This indicates a large change in the distribution of the Ca II ion depending on the depth of the ejecta.

4. PROPERTIES OF SUPERNOVA LINE POLARIZATION

4.1. Ubiquity of Non-axisymmetry

In Table 2, we summarize line polarization measurements obtained so far for stripped-envelope SNe. Here the line polarization is defined as a relative change from the continuum level, and thus, not affected by the ISP. We show six stripped-envelope SNe with high-quality data, namely, Type Ib SNe 2005bf (Maund et al. 2007b; Tanaka et al. 2009a), 2008D (Maund et al. 2009), 2009jf (this paper), Type Ic SNe 2002ap (Kawabata et al. 2002; Leonard et al. 2002; Wang et al. 2003b), 2007gr (Tanaka et al. 2008), and 2009mi (this paper). As also noted by Wang & Wheeler (2008), it is clear that all SNe show non-zero polarization, which means that stripped-envelope SNe generally have asymmetric explosion geometry.

For SNe 2005bf and 2008D, Maund et al. (2007b, 2009) found a loop in the $Q-U$ diagram at strong lines, which is indicative of a 3D geometry (Kasen et al. 2003; Maund et al. 2007b, 2007c; see also Figure 2). Our new data for SNe 2009jf and 2009mi also show a loop in the $Q-U$ diagram. We have checked the literature about SN 2002ap (Kawabata et al. 2002; Leonard et al. 2002; Wang et al. 2003b). Although they do not explicitly mention the loop, the data in Kawabata et al. (2002)

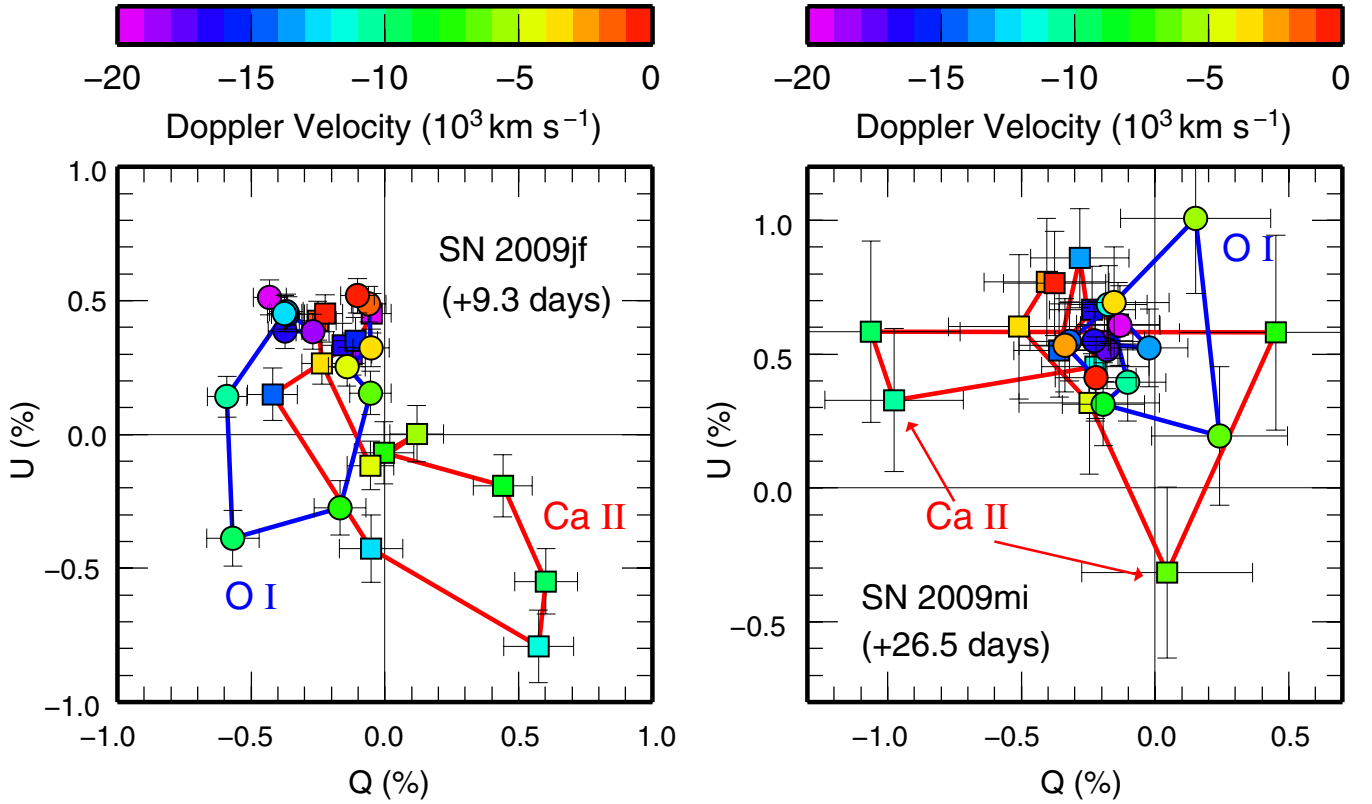


Figure 5. Observed polarization data of SNe 2009jf (left) and 2009mi (right) around the O I line (circles connected with the blue line) and Ca II line (squares connected with the red line). The polarization data are binned into 50 \AA , giving a velocity resolution of about 1900 and 1700 km s^{-1} for the O I and Ca II lines, respectively. The interstellar polarization is *not* corrected for. Different colors represent different Doppler velocities as shown in the color bar above the plots. Although the Ca II triplet seems to be resolved in the total flux of SNe 2009jf and 2009mi (Figure 3), the velocity in this figure is simply measured from the mean wavelength (8567 \AA). In our data, there is no evidence for an additional high-velocity component of the Ca II line as seen in some other SNe (see, e.g., Maund et al. 2009). The O I and Ca II features show a loop in the $Q-U$ plane, indicating non-axisymmetric distribution. In addition, the Ca II line in SN 2009mi shows a large change of the angle measured from the reference point.

(A color version of this figure is available in the online journal.)

Table 2
Summary of Line Polarization

Object	Type	3D?	Epoch (day)	P_{FeII} (%)	P_{CaII} (%)	P_{OI} (%)	$P_{\text{NaI/HeI}}$ (%)	FD_{FeII}	FD_{CaII}	FD_{OI}	$\text{FD}_{\text{NaI/HeI}}$	Ref.
SN 2005bf	Ib	Yes	-6	0.8 (0.2)	3.5 (0.5)	0.0 (0.3)	1.2 (0.2)	0.37 (0.03)	0.50 (0.05)	0.0 (0.0)	0.40 (0.03)	1
			8	0.4 (0.2)	1.5 (0.3)	0.0 (0.5)	0.6 (0.4)	0.21 (0.02)	0.39 (0.02)	0.0 (0.0)	0.46 (0.02)	2
SN 2008D	Ib	Yes	3.3	0.8 (0.2)	1.8 (0.3)	0.5 (0.13)	0.4 (0.2)	0.35 (0.03)	0.49 (0.02)	0.23 (0.03)	0.46 (0.02)	3
			18.3	1.0 (0.3)	2.5 (0.7)	0.3 (0.13)	1.1 (0.1)	0.50 (0.05)	0.58 (0.05)	0.24 (0.02)	0.58 (0.02)	3
SN 2009jf	Ib	Yes	9.3	0.4 (0.2)	1.2 (0.2)	0.9 (0.2)	0.5 (0.2)	0.32 (0.03)	0.69 (0.02)	0.38 (0.02)	0.38 (0.02)	This paper
SN 2002ap	Ic	Yes	1	0.18 (0.05)	...	0.8 (0.1)	0.0 (0.05)	0.20 (0.03)	...	0.38 (0.02)	0.04 (0.02)	4,5
			3	0.12 (0.05)	...	0.6 (0.1)	0.0 (0.1)	0.21 (0.03)	...	0.34 (0.02)	0.04 (0.02)	4,5
			6	0.0 (0.1)	0.3 (0.1)	0.5 (0.1)	0.0 (0.1)	0.27 (0.05)	0.36 (0.05)	0.50 (0.05)	0.06 (0.02)	6
			27	...	1.6 (0.1)	0.0 (0.2)	0.2 (0.1)	...	0.65 (0.04)	0.41 (0.05)	0.31 (0.03)	4
SN 2007gr	Ic	No	21	0.0 (0.3)	2.5 (0.3)	0.0 (0.3)	0.0 (0.3)	0.42 (0.03)	0.88 (0.02)	0.56 (0.02)	0.65 (0.02)	7
SN 2009mi	Ic	Yes	26.5	0.5 (0.2)	0.9 (0.2)	0.5 (0.2)	0.0 (0.2)	0.41 (0.04)	0.83 (0.02)	0.56 (0.02)	0.46 (0.02)	This paper

References. (1) Maund et al. 2007b; (2) Tanaka et al. 2009a; (3) Maund et al. 2009; (4) Kawabata et al. 2002; (5) Wang et al. 2003b; (6) Leonard et al. 2002; (7) Tanaka et al. 2008.

show a loop in the Ca II line. Thus, loops are quite common in stripped-envelope SNe; five of six stripped-envelope SNe show the loop. This implies that a non-axisymmetric, 3D geometry is common in stripped-envelope SNe.

4.2. Relation between Line Polarization and Absorption Depth

Figure 6 shows the observed line polarization as a function of epoch from maximum brightness. There is a large variety in the polarization degree. It is clear that the Ca II line (blue)

tends to be more polarized than the other lines. There is no clear trend in the time evolution; the line polarization could increase or decrease with time.

Figure 7 shows the same polarization data as a function of the fractional depth (FD) of the absorption. The FD is defined as

$$\text{FD} = \frac{F_{\text{cont}} - F_{\text{abs}}}{F_{\text{cont}}}, \quad (3)$$

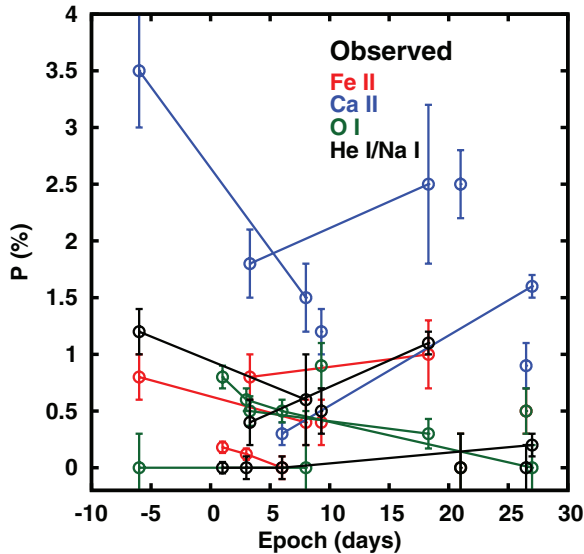


Figure 6. Observed line polarization as a function of SN epoch. Data for the same SN are connected with lines. There is no clear trend in the time evolution of the line polarization. The Ca II line tends to be more polarized than the other lines.

(A color version of this figure is available in the online journal.)

where F_{cont} and F_{abs} are the fluxes at the continuum and absorption minimum, respectively.

Figure 7 shows that stronger lines tend to show a higher polarization degree. In fact, there are no observational points at the top left of the plot, i.e., $\text{FD} < 0.3$ and $P_{\text{obs}} > 1\%$. This seems natural because the absorption, unless it is quite strong, cannot cause a significant incomplete cancellation of the polarization (Figure 1).

We can analyze this relation in a simple, analytic way. We assume a spherical photosphere projecting an area S on the sky. Within this photospheric disk, the flux per unit area I and the polarization degree are assumed to be uniform. The total flux from the photospheric disk is $F_{\text{cont}} = IS$. When light is emitted from a point on the photospheric disk on the sky, it can undergo line absorption with an absorption fraction $x_{\text{abs}} \equiv 1 - \exp(-\tau)$. At the wavelength of this line, the flux is $F_{\text{abs}} = (1 - x_{\text{abs}})IS$.

If the distribution of the line opacity is uniform, no polarization is expected at the line, i.e., $P_{\text{abs}} = 0$ (Section 1.2). To introduce asymmetry in the line opacity, we assume that the absorption fraction is enhanced by a factor of f in a region ΔS (e.g., the shaded region in Figure 1(c)). Then, the total flux at the wavelength of the line is

$$\begin{aligned} F_{\text{abs}} &= (1 - x_{\text{abs}})I(S - \Delta S) + (1 - fx_{\text{abs}})I\Delta S \\ &= [(1 - x_{\text{abs}}) - (f - 1)x_{\text{abs}}\Delta S/S]IS, \end{aligned} \quad (4)$$

and the FD (Equation (3)) can be written by using Equation (4) as

$$\text{FD} = x_{\text{abs}} + (f - 1)x_{\text{abs}}\Delta S/S. \quad (5)$$

The asymmetry introduced above results in an incomplete cancellation of the polarization. If this region has a constant polarization direction, the amount of non-canceled flux is equivalent to the excess absorption in the region, i.e.,

$$P_{\text{abs}}F_{\text{abs}} = (f - 1)x_{\text{abs}}I\Delta S. \quad (6)$$

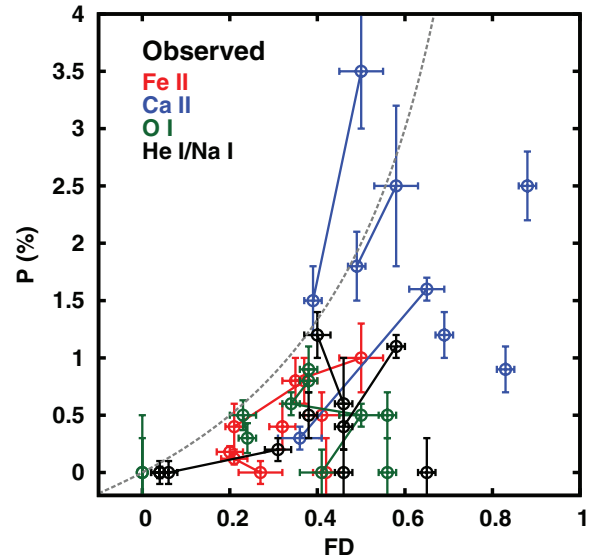


Figure 7. Observed line polarization as a function of fractional depth of the absorption. Data for the same SN are connected with lines. There is a general trend that stronger lines show higher polarization. The gray dashed line shows the line polarization expected from Equation (8) for the case of $P_{\text{cor}} = 2.0\%$.

(A color version of this figure is available in the online journal.)

Then, the polarization degree can be expressed as a function of the FD:

$$P_{\text{abs}} = \frac{(f - 1)x_{\text{abs}}\Delta S/S}{1 - \text{FD}}. \quad (7)$$

Unless the enhanced opacity dominates the absorption, $\text{FD} \simeq x_{\text{abs}}$ (Equation (5)). Thus,

$$P_{\text{abs}} \simeq (f - 1)\Delta S/S \frac{\text{FD}}{1 - \text{FD}} = P_{\text{cor}} \frac{\text{FD}}{1 - \text{FD}}, \quad (8)$$

where we define a corrected polarization degree $P_{\text{cor}} \equiv (f - 1)\Delta S/S$. This corrected polarization degree is equivalent to the polarization with $\text{FD} = 0.5$. It can be interpreted as a rough indicator of the product of the amount of the enhancement $(f - 1)$ and the fractional area of the enhanced region $\Delta S/S$ under the assumption that the enhanced region only has one polarization direction. The gray dashed line in Figure 7 shows the line polarization expected from Equation (8) with $P_{\text{cor}} = 2.0\%$.

Note that the analytic equations here involve significant simplifications, i.e., a constant intensity in the photospheric disk and a constant direction of polarization in the enhanced region. But if we use ΔS as an intensity-weighted area, in which polarization is not canceled, the equation holds even for general cases with a non-constant intensity and many opacity-enhanced regions.

From Equation (8), it is expected that stronger lines with a larger FD tend to have higher polarization, which is actually found in Figure 7. It should be emphasized that the variety of the observed line polarization is largely generated by a variety of the absorption depth. The absorption depth is primarily determined by the density, chemical abundance, or ionization in the ejecta, which can be varied even in the 1D explosion (reflecting the mass and kinetic energy of the ejecta, and the temperature in the ejecta).

Figure 8 shows the observed polarization (left) and polarization corrected for the absorption depth (right) for each stripped-envelope SN. It is obvious that after correcting for the absorption depth, the Ca II line is not always more polarized than the other

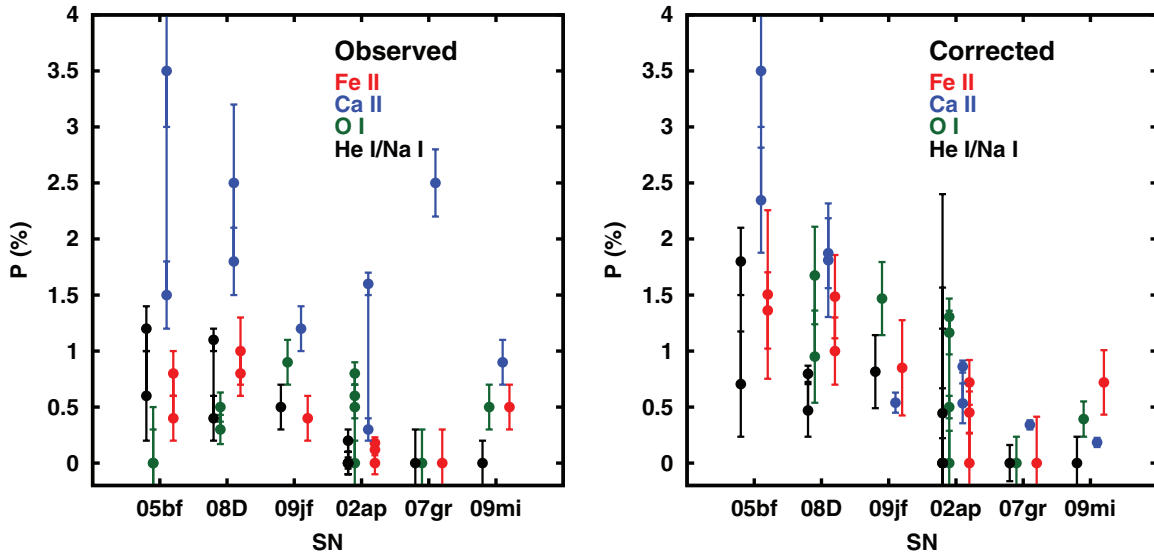


Figure 8. Left: observed line polarization for stripped-envelope SNe. The Ca II line is usually more polarized than the other lines. Right: line polarization corrected for the absorption depth (Equation (8)). After correcting for the effect of the absorption depth, the Ca II line is not always more polarized than the other lines. (A color version of this figure is available in the online journal.)

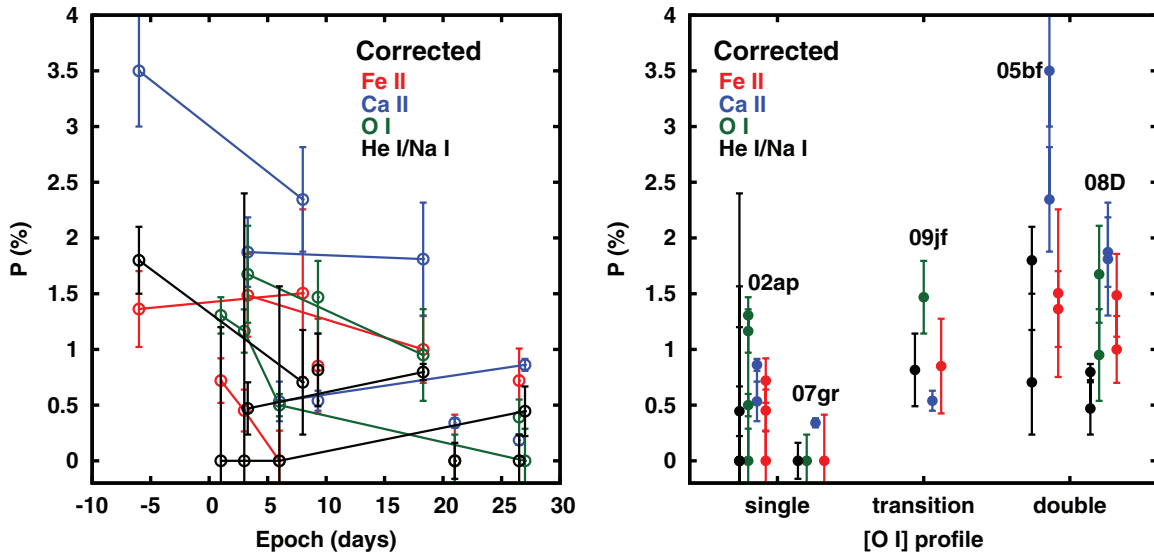


Figure 9. Left: corrected line polarization as a function of SN epoch. Data for the same SN are connected with lines. Right: relation between the corrected line polarization and the nebular [O I] line profile. (A color version of this figure is available in the online journal.)

lines. This demonstrates the importance of the correction. To compare the polarization of different lines or different objects correctly, one must correct for this effect, which is not directly related to the geometry. This fact has been overlooked in previous analyses. It would be interesting to study this effect also on the line polarization of Type Ia SNe, which has been suggested to be correlated to the declining rate of the light curve (Wang et al. 2007).

4.3. Properties of Corrected Polarization

It is clear that there is a remaining dispersion in the line polarization among different objects even after correcting for the absorption depth (right panel in Figure 8). We first examine if the corrected polarization is related with the epoch. The left panel of Figure 9 shows the corrected line polarization as a function of epoch. Although there is a weak trend of the polarization

decreasing with time, it is not clear if all the variety in the corrected polarization can be explained by the effect of the epoch.

The remaining dispersion could also be understood by the multi-dimensional properties of each SN. It is thus worth studying the relationship between the line polarization and the [O I] line profile in the nebular spectra, which is another geometric probe of the SN ejecta (Mazzali et al. 2001, 2005; Maeda et al. 2002, 2008; Modjaz et al. 2008; Tanaka et al. 2009b; Taubenberger et al. 2009; Maurer et al. 2010).

The right panel of Figure 9 shows the relation between the corrected line polarization and the [O I] line profile. SNe 2002ap and 2007gr show a single-peak profile (Leonard et al. 2002; Foley et al. 2003; Mazzali et al. 2007, 2010; Hunter et al. 2009) while SNe 2005bf and 2008D show a double-peak profile (Maeda et al. 2007; Modjaz et al. 2009; Tanaka et al. 2009b). The [O I] profile of SN 2009jf is complex; it shows both

single- and double-peak components (Sahu et al. 2011; Valenti et al. 2011). Following the classification by Maeda et al. (2008), we classify it as “transition.” With only five objects, it is difficult to draw a firm conclusion. It is therefore important to increase spectropolarimetric samples to further study this relation.

The dispersion may also reflect a difference between Type Ib and Ic. In fact, three Type Ic SNe in our sample tend to have a lower polarization degree than three Type Ib SNe (left panel of Figure 8). By increasing the number of samples, we will be able to study the effect of the existence of the He envelope on the explosion geometry.

One natural scenario is that the dispersion is caused by random line-of-sight effects. As discussed in Section 4.1, stripped-envelope SNe generally have a 3D geometry. If we assume a clumpy structure as in the left bottom panel of Figure 2, a variety of polarization is naturally expected for different lines of sight. Since the effect of the line of sight is very sensitive to the size and the number of clumps, it can be used as an observational probe to study a typical 3D geometry of SNe. This will be further studied in a forthcoming paper.

5. CONCLUSIONS

We have performed spectropolarimetric observations of two stripped-envelope SNe, Type Ib SN 2009jf and Type Ic SN 2009mi. Both objects show non-zero line polarization at the wavelength of strong absorption lines. The polarization data show a “loop” in the $Q-U$ diagram, which indicates a non-axisymmetric, 3D distribution of ions in the SN ejecta. After adding our new data to the sample of stripped-envelope SNe with high-quality spectropolarimetric observations, five SNe out of six show a loop in the $Q-U$ diagram. We conclude that a non-axisymmetric, 3D geometry is common in stripped-envelope SNe.

We have studied the properties of line polarization in stripped-envelope SNe. We have found that a stronger line tends to show a higher polarization. We give an analytic equation that naturally explains this relation. Although the Ca II line usually shows a higher line polarization than the other lines, it is not always true after correcting for the absorption depth. This effect must be corrected in order to compare the polarization of different lines or different objects.

Even after correcting for the absorption depth, there is a dispersion in the polarization degree among different objects. This dispersion could simply reflect the epoch of the observations. It might also be related to the [O I] line profile in the nebular spectra or SN types (Type Ib or Ic), although it is not possible to draw any firm conclusion with the current sample. Also, if we assume a 3D clumpy structure, the variety is naturally expected from the line-of-sight effect. Modeling of spectropolarimetric data will be performed in a forthcoming paper.

We are grateful to the staff and observers of the Subaru Telescope, especially Masahiko Hayashi and Hiroshi Terada for their effort on the time allocation of our ToO observations in 2009. M.T. thanks Yudai Suwa and Takami Kuroda for valuable comments. This research has been supported by the Grant-in-Aid for Scientific Research of the Japan Society for the Promotion of Science (22840009, 24740117) and by World Premier International Research Center Initiative, MEXT, Japan. This research has made use of the SUSPECT (<http://suspect.nhn.ou.edu/~suspect/>), the Online Supernova Spectrum Archive at the Department of Physics and Astronomy, University of Oklahoma.

REFERENCES

- Blondin, J. M., Mezzacappa, A., & DeMarino, C. 2003, *ApJ*, 584, 971
 Buras, R., Rampp, M., Janka, H.-T., & Kifonidis, K. 2006, *A&A*, 447, 1049
 Burbidge, E. M., Burbidge, G. R., Fowler, W. A., & Hoyle, F. 1957, *Rev. Mod. Phys.*, 29, 547
 Burrows, A., Hayes, J., & Fryxell, B. A. 1995, *ApJ*, 450, 830
 Chornock, R., & Filippenko, A. V. 2008, *AJ*, 136, 2227
 Chornock, R., Filippenko, A. V., Li, W., et al. 2011, *ApJ*, 739, 41
 Chornock, R., Filippenko, A. V., Li, W., & Silverman, J. M. 2010, *ApJ*, 713, 1363
 Colgate, S. A., & White, R. H. 1966, *ApJ*, 143, 626
 DeLaney, T., Rudnick, L., Stage, M. D., et al. 2010, *ApJ*, 725, 2038
 Foglizzo, T., Galletti, P., Scheck, L., & Janka, H.-T. 2007, *ApJ*, 654, 1006
 Foley, R. J., Papenkova, M. S., Swift, B. J., et al. 2003, *PASP*, 115, 1220
 Fujimoto, S.-i., Kotake, K., Hashimoto, M.-a., Ono, M., & Ohnishi, N. 2011, *ApJ*, 738, 61
 Hanke, F., Marek, A., Mueller, B., & Janka, H.-T. 2011, arXiv:1108.4355
 Herant, M., Benz, W., Hix, W. R., Fryer, C. L., & Colgate, S. A. 1994, *ApJ*, 435, 339
 Höflich, P. 1991, *A&A*, 246, 481
 Hole, K. T., Kasen, D., & Nordsieck, K. H. 2010, *ApJ*, 720, 1500
 Hunter, D. J., Valenti, S., Kotak, R., et al. 2009, *A&A*, 508, 371
 Isensee, K., Rudnick, L., DeLaney, T., et al. 2010, *ApJ*, 725, 2059
 Iwakami, W., Kotake, K., Ohnishi, N., Yamada, S., & Sawada, K. 2008, *ApJ*, 678, 1207
 Janka, H.-T., & Mueller, E. 1996, *A&A*, 306, 167
 Jeffery, D. J. 1989, *ApJS*, 71, 951
 Kasen, D., Nugent, P., Wang, L., et al. 2003, *ApJ*, 593, 788
 Kashikawa, N., Aoki, K., Asai, R., et al. 2002, *PASJ*, 54, 819
 Kasliwal, M. M., Howell, J. L., Fox, D. B., Quimby, R., & Gal-Yam, A. 2009, *CBET*, 1955, 1
 Kawabata, K. S., Jeffery, D. J., Iye, M., et al. 2002, *ApJ*, 580, L39
 Kifonidis, K., Plewa, T., Janka, H.-T., & Müller, E. 2000, *ApJ*, 531, L123
 Kifonidis, K., Plewa, T., Janka, H.-T., & Müller, E. 2003, *A&A*, 408, 621
 Kinugasa, K., Honda, S., Takahashi, H., & Taguchi, H. 2009, *CBET*, 2082, 1
 Kjær, K., Leibundgut, B., Fransson, C., Jerkstrand, A., & Spyromilio, J. 2010, *A&A*, 517, A51
 Kuroda, T., Kotake, K., & Takiwaki, T. 2012, arXiv:1202.2487
 Leonard, D. C., & Filippenko, A. V. 2005, in ASP Conf. Ser. 342, 1604-2004: Supernovae as Cosmological Lighthouses, ed. M. Turatto, S. Benetti, L. Zampieri, & W. Shea (San Francisco, CA: ASP), 330
 Leonard, D. C., Filippenko, A. V., Chornock, R., & Foley, R. J. 2002, *PASP*, 114, 1333
 Leonard, D. C., Filippenko, A. V., Ganeshalingam, M., et al. 2006, *Nature*, 440, 505
 Leonard, D. C., Li, W., Filippenko, A. V., Foley, R. J., & Chornock, R. 2005, *ApJ*, 632, 450
 Li, W., Cenko, S. B., & Filippenko, A. V. 2009, *CBET*, 1952, 1
 Liebendörfer, M., Mezzacappa, A., Thielemann, F.-K., et al. 2001, *Phys. Rev. D*, 63, 103004
 Maeda, K., Kawabata, K., Mazzali, P. A., et al. 2008, *Science*, 319, 1220
 Maeda, K., Mazzali, P. A., Deng, J., et al. 2003, *ApJ*, 593, 931
 Maeda, K., Nakamura, T., Nomoto, K., et al. 2002, *ApJ*, 565, 405
 Maeda, K., Tanaka, M., Nomoto, K., et al. 2007, *ApJ*, 666, 1069
 Marek, A., & Janka, H.-T. 2009, *ApJ*, 694, 664
 Massey, P., & Gronwall, C. 1990, *ApJ*, 358, 344
 Massey, P., Strobel, K., Barnes, J. V., & Anderson, E. 1988, *ApJ*, 328, 315
 Maund, J. R., Wheeler, J. C., Baade, D., et al. 2009, *ApJ*, 705, 1139
 Maund, J. R., Wheeler, J. C., Patat, F., et al. 2007a, *A&A*, 475, L1
 Maund, J. R., Wheeler, J. C., Patat, F., et al. 2007b, *MNRAS*, 381, 201
 Maund, J. R., Wheeler, J. C., Patat, F., et al. 2007c, *ApJ*, 671, 1944
 Maurer, J. I., Mazzali, P. A., Deng, J., et al. 2010, *MNRAS*, 402, 161
 Mazzali, P. A., Kawabata, K. S., Maeda, K., et al. 2005, *Science*, 308, 1284
 Mazzali, P. A., Kawabata, K. S., Maeda, K., et al. 2007, *ApJ*, 670, 592
 Mazzali, P. A., Maurer, J. I., Valenti, S., Kotak, R., & Hunter, D. 2010, *MNRAS*, 408, 87
 Mazzali, P. A., Nomoto, K., Patat, F., & Maeda, K. 2001, *ApJ*, 559, 1047
 Milisavljevic, D., Fesen, R. A., Gerardy, C. L., Kirshner, R. P., & Challis, P. 2010, *ApJ*, 709, 1343
 Modjaz, M., Kirshner, R. P., Blondin, S., Challis, P., & Matheson, T. 2008, *ApJ*, 687, L9
 Modjaz, M., Li, W., Butler, N., et al. 2009, *ApJ*, 702, 226
 Monard, L. A. G., Africa, S., & Brimacombe, J. 2009, *CBET*, 2077, 1

- Nagataki, S., Hashimoto, M.-A., Sato, K., & Yamada, S. 1997, *ApJ*, **486**, 1026
- Nordhaus, J., Burrows, A., Almgren, A., & Bell, J. 2010, *ApJ*, **720**, 694
- Ohnishi, N., Kotake, K., & Yamada, S. 2006, *ApJ*, **641**, 1018
- Oke, J. B. 1990, *AJ*, **99**, 1621
- Patat, F., Baade, D., Höflich, P., et al. 2009, *A&A*, **508**, 229
- Rampp, M., & Janka, H.-T. 2000, *ApJ*, **539**, L33
- Sahu, D. K., Anupama, G. C., & Gurugubelli, U. K. 2009, *CBET*, **1955**, 2
- Sahu, D. K., Gurugubelli, U. K., Anupama, G. C., & Nomoto, K. 2011, *MNRAS*, **413**, 2583
- Scheck, L., Plewa, T., Janka, H.-T., Kifonidis, K., & Müller, E. 2004, *Phys. Rev. Lett.*, **92**, 011103
- Schmidt, G. D., Elston, R., & Lupie, O. L. 1992, *AJ*, **104**, 1563
- Serkowski, K., Mathewson, D. L., & Ford, V. L. 1975, *ApJ*, **196**, 261
- Shapiro, P. R., & Sutherland, P. G. 1982, *ApJ*, **263**, 902
- Sumiyoshi, K., Yamada, S., Suzuki, H., et al. 2005, *ApJ*, **629**, 922
- Suwa, Y., Kotake, K., Takiwaki, T., et al. 2010, *PASJ*, **62**, L49
- Takiwaki, T., Kotake, K., & Suwa, Y. 2012, *ApJ*, **749**, 98
- Tanaka, M., Kawabata, K. S., Maeda, K., et al. 2009a, *ApJ*, **699**, 1119
- Tanaka, M., Kawabata, K. S., Maeda, K., Hattori, T., & Nomoto, K. 2008, *ApJ*, **689**, 1191
- Tanaka, M., Maeda, K., Mazzali, P. A., & Nomoto, K. 2007, *ApJ*, **668**, L19
- Tanaka, M., Yamanaka, M., Maeda, K., et al. 2009b, *ApJ*, **700**, 1680
- Taubenberger, S., Valenti, S., Benetti, S., et al. 2009, *MNRAS*, **397**, 677
- Thompson, T. A., Burrows, A., & Pinto, P. A. 2003, *ApJ*, **592**, 434
- Tinbergen, J. 1996, *Astronomical Polarimetry* (Cambridge: Cambridge Univ. Press)
- Tominaga, N. 2009, *ApJ*, **690**, 526
- Turnshek, D. A., Bohlin, R. C., Williamson, R. L., II, et al. 1990, *AJ*, **99**, 1243
- Valenti, S., Fraser, M., Benetti, S., et al. 2011, *MNRAS*, **416**, 3138
- Wang, L., Baade, D., Höflich, P., et al. 2003a, *ApJ*, **591**, 1110
- Wang, L., Baade, D., Höflich, P., et al. 2006, *ApJ*, **653**, 490
- Wang, L., Baade, D., Höflich, P., & Wheeler, J. C. 2003b, *ApJ*, **592**, 457
- Wang, L., Baade, D., & Patat, F. 2007, *Science*, **315**, 212
- Wang, L., & Wheeler, J. C. 2008, *ARA&A*, **46**, 433
- Wang, L., Wheeler, J. C., Höflich, P., et al. 2002, *ApJ*, **579**, 671
- Wongwathanarat, A., Janka, H.-T., & Müller, E. 2010, *ApJ*, **725**, L106